Paper presented at the Nuclear Science Symposium
Medical Imaging Conference, Norfolk, Oct. 30-Nov. 5

TRI-PP-94-81
Oct 1994

CA9600458

Design Studies of a Depth Encoding Large Aperture PET Camera

C. Moisan, J. G. Rogers, K. R. Buckley, T. J. Ruth, M. W. Stazyk, and G. Tsang
TRIUMF, 4004 Wesbrook Mall, Vancouver B.C., Canada V6T 2A3

to be submitted to IEEE Transactions on Nuclear Science

Abstract

The feasibility of a wholebody PET tomograph with the capacity to correct for the parallax error induced by the Depth-Of-Interaction of γ-rays is assessed through simulation. The experimental energy, depth, and transverse position resolutions of BGO block detector candidates are the main inputs to a simulation that predicts the point source resolution of the Depth Encoding Large Aperture Camera (DELAC). The results indicate that a measured depth resolution of 7 mm (FWHM) is sufficient to correct a substantial part of the parallax error for a point source at the edge of the Field-Of-View. A search for the block specifications and camera ring radius that would optimize the spatial resolution and its uniformity across the Field-Of-View is also presented.

I. Introduction

In modern PET cameras a large ring diameter is required for good resolution so that impinging γ-ray trajectories are parallel to the long axis of small detector crystals. When imaging point sources away from the center of the Field-Of-View (FOV), trajectories depart significantly from this ideal and the image is increasingly blurred. This effect, commonly referred to as a parallax error, causes the projection of a point source at the edge of the FOV to be shifted and skewed toward the center. Knowledge of the Depth-Of-Interaction (DOI) of the γ's allows for a correction of this error and improves the image resolution uniformity across the tomograph FOV. Recent work by Rogers [1] indicates that an improved DOI resolution can be obtained if the light collection efficiency of the detector is depth dependent. The development of DOI sensitive detectors hence opens the potential for smaller ring diameter scanners. This will lead to the possibility to build scanners with better image resolution and sensitivity at lower cost.

In this context, the design of a new wholebody PET tomograph with the capacity to correct for DOI blurring is under study at TRIUMF. Leading studies for the DELAC project are aimed at three goals:

- to experimentally demonstrate the ability to determine the DOI in practical γ-ray detectors, based on light collection, without spoiling the transverse position resolution,
- to simulate the correction of the parallax error in a positron volume imaging tomograph using the measured performance of such DOI sensitive blocks, and
- to determine the limits of the parallax correction given different block candidates' geometry and projected DOI resolution.

Initially, the attention has therefore focussed on the impact of measured BGO detector performances on the DELAC image resolution. The experimental energy and DOI resolutions as well as the Line-Spread-Functions (LSF) of existing BGO block detectors are the main inputs to a simulation that predicts the DELAC resolution. This approach ensures the reliability of preliminary results while avoiding extensive modelling of the light transport in DOI sensitive blocks.

II. Block performance measurements

A. Block Candidate Specifications

Initial studies are based on measurements taken with two candidate BGO block detectors. Both new blocks are modified versions of the standard commercial detectors manufactured by Siemens-CTI as already described in [2]. The first new candidate has dimensions $50\times54\times30$ mm^3 with 12×12 crystal segmentation, and is termed the "large 12×12" block. The light yield from interacting γ-rays is read by a conventional assembly of four photomultipliers coupled to the back face of the BGO block. Given that each quadrant of the block is read by one of the PMT's, the granularity of the block can be characterized by its crystal to quadrant surface ratio of 1/36. The block had been previously altered to induce a sensitivity to the incident γ-rays' DOI. This was achieved by modifying the standard

surface treatment of the crystals such that shallow interactions appear dimmer than usual due to a gradient in the light collection efficiency.

The second block candidate has dimensions of $36\times38\times30$ mm^3 with an 8×8 segmentation, and is termed the "small 8×8" block. The standard surface treatment of that block was not yet altered. Four PMT's read out the block as in the previous case. The block nevertheless presents a coarser segmentation with a crystal to quadrant surface ratio of 1/16. Crystals are approximatively of 4.5×4.5 mm^2 in both block candidates, but the coarser segmentation of the small 8×8 block should result in an improved position resolution compared to that of the large 12×12.

B. Experimental Configuration

For these studies, 511 keV γ-rays from a 0.3 mCi source of ^{68}Ge were used in a benchtop setup described in detail in [2]. To minimize scatter, data was taken in coincidence mode, using a conjugate detector at a distant position on the opposite side of the source. To avoid the contribution of the conjugate detector's position resolution, the source was collimated with lead bricks to achieve two different beam profiles at the front face of the block candidate under study.

A fan beam was obtained by using two 5 cm thick lead bricks separated by a 1 mm slit. The detector under study was positioned close behind the bricks while the source was at a distance of typically 10 cm from the bricks.

A pencil beam was formed by placing the same source behind a 8 cm long hole of 2.7 mm diameter drilled in a lead brick. At the position occupied by the detector, the full-width-at-half-maximum (FWHM) of the beam was measured to be $\sim$4 mm.

The sum of the four PMT signals, $(A+B+C+D)$, was thresholded and used to drive the coincidence trigger logic. The signal from each PMT was acquired from a 10-bit ADC. The four ADC conversions were available for subsequent offline processing.

C. Position Reconstruction

The position of a given γ-ray interaction in the transverse (X,Y) plane of the block, is estimated from the PMT signals according to:

$$X_m = \frac{(B+D)-(A+C)}{A+B+C+D} \quad (1)$$

$$Y_m = \frac{(A+B)-(C+D)}{A+B+C+D}. \quad (2)$$

A lookup table is necessary to relate a given (X_m, Y_m) pair to a crystal address as the relationship between measured and true interaction positions is typically non-linear in such BGO block detectors [2, 3].

D. Measuring the DOI Response

The DOI response of the large 12×12 block was measured according to the method recently presented by Rogers [1]. The data were obtained by shining the fan beam at six different depths on the side face of the block. The variation of the photopeak ADC channel, E, is shown as a function of the DOI, Z, in Figure 1. The depth response is shown separately for γ-rays interacting in five selected crystals taken along the diagonal of one quadrant of the block face. Given a specific crystal, the depth dependence of the photopeak channel proves to be linear to a good approximation. Furthermore, the slope of the depth response curve stays constant to within $\pm5\%$ for all considered crystals.

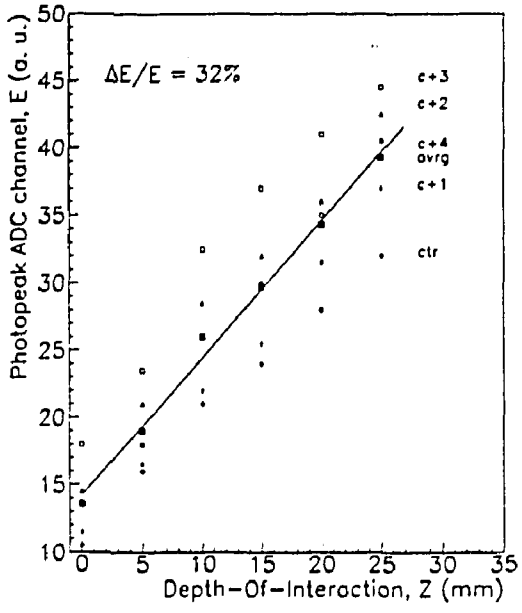

Figure 1: Measured DOI response of the large 12×12 block detector given by the photopeak ADC channel, E, as a function of the DOI, Z, of 511 keV photons. The various small open symbols show the response of different crystals taken along the diagonal of one detector quadrant. The large full squares show the average response that is fitted by a linear function.

As indicated by the uniform slopes among the individual crystals, the depth response of the block may be considered independent of the measured γ-ray interaction position in the (X,Y) plane. Averaging the photopeak ADC channel over the various crystals as a function of depth then provides a crystal-independent DOI response function which is shown on Figure 1 by the full squares. A fit of that average to a linear function is given by the full line.

The variation with depth of the light collection efficiency in the block is expressed by the "DOI sensitivity": S_{DOI}. It is calculated as a fraction or percentage from the photopeak ADC channel at minimum and maximum depths,

$E(0)$ and $E(z_{block})$:

$$S_{DOI} = \frac{E(z_{block}) - E(0)}{\max(E(z_{block}), E(0))}, \quad (3)$$

where, z_{block} is the block thickness. From the previous equation and the average fit in Figure 1, S_{DOI} = 68% for the large 12×12 block. This implies that interactions occurring at the front face of the block are 68% dimmer than those that happen at the surface near the PMT's.

It is also convenient to introduce the "photon fractional loss":

$$L(Z) = \frac{\max(E(z_{block}), E(0)) - E(Z)}{\max(E(z_{block}), E(0))}, \quad (4)$$

$$= 1 - S_{DOI}\frac{E(Z)}{E(z_{block}) - E(0)}. \quad (5)$$

As defined, L is a measure, at a given depth, of the fraction of the deposited energy that is lost due to the depth dependence of the light collection efficiency in the block.

The resolution on the measured DOI, ΔZ, follows from the ratio of the photopeak energy resolution to the slope of the DOI response function of the block, (dE/dZ). Since the energy resolution varies with depth, ΔZ is itself a function of the DOI. The following equations allow its evaluation:

$$\Delta Z(Z) = \frac{(\Delta E/E)\,E(Z)}{(dE/dZ)}, \quad (6)$$

$$= \frac{(\Delta E/E)\,(1 - L(Z))}{S_{DOI}/z_{block}}, \quad (7)$$

where $\Delta E/E$ is the measured photopeak energy resolution. To represent the block performance as a whole, $\Delta E/E$, ΔZ and L are evaluated at the median depth, z_m, by which half of the detected γ-rays have already interacted. For the large 12×12 block, z_m=7.9 mm, $\Delta E/E$=32% (FWHM), and L=50%. Expression (7) then leads to a DOI resolution of 7 mm at the median depth.

E. Transverse Position Resolution

The transverse Line-Spread-Functions (LSF's) of both block candidates were first measured by stepping the fan beam across the front face of the detector. The response of each crystal along one axis of the block was measured by counting the number of γ-rays detected in that crystal as a function of the fan beam slit position relative to the center of that crystal. Steps of 1 mm were used to completely scan the face of the block. The response was averaged along the axis of the block parallel to the slit.

Figure 2(a) presents the LSF obtained with the fan beam for a column of crystals at the center of the large 12×12 block. The crystal response shows a FWHM of 5 mm. This value is mostly determined by its physical size. The FWTM of the LSF is noticeably poor due to side-lobes appearing at the positions of adjacent crystals. This position miscoding can be attributed to the independent or joint effects of two features of the block: its high segmentation or its previous alteration to obtain DOI sensitivity which was accomplished at the cost of a lower light collection efficiency. Gamma-ray scattering may also contribute significantly to the tails of the distribution. Further measurements were taken on the small 8×8 block, prior to modifying it for DOI sensitivity, to assess which of these dominates the resolution.

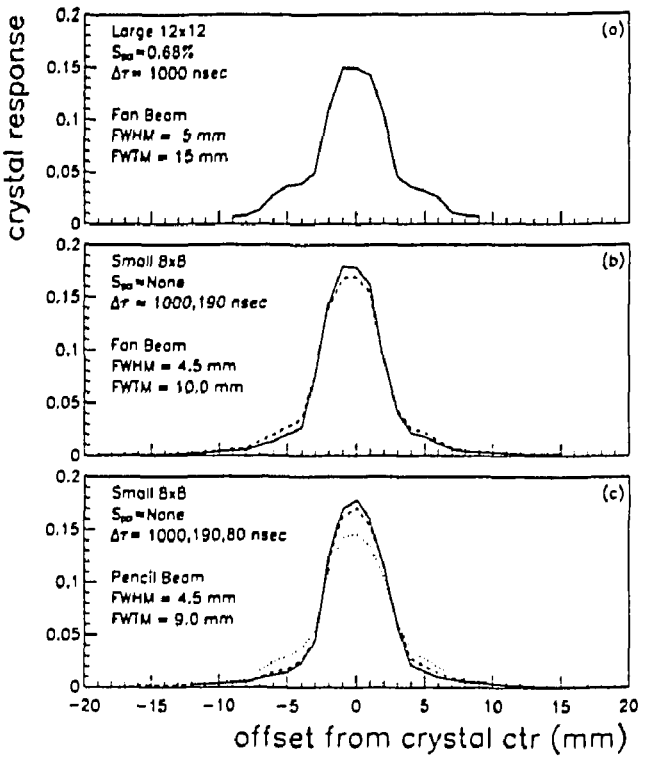

Figure 2: Measured transverse Line-Spread-Functions for a column of crystals at the center of block detectors. (a) For the large 12×12 block with the fan beam and an ADC integration time, $\Delta\tau$, of 1000 nsec. (b) For the small 8×8 block with the fan beam and ADC integration times of 1000 (full line) and 190 nsec (long dashes). (c) Again for the small 8×8 block with the pencil beam and an ADC integration times of 1000 (full line), 190 (dashed line) and 80 nsec (dotted line).

When measuring the large 12×12 LSF's, the width of the ADC integration time, $\Delta\tau$, was initially set to a value of 1000 nsec to collect all the light reaching the PMT's. In subsequent measurements with the small 8×8 block, $\Delta\tau$ was varied to imitate a lossy crystal reflecting coating [4]. Reduced light collection was obtained by shortening the ADC integration gate time to ignore controlled fractions, L, of photons detected in the PMT's. The ADC gate was closed at a fixed time delay after the start of scintillation as measured by the constant fraction discriminator [2]. The times to respectively obtain L=50% and L=75% were determined to be 190 nsec and 80 nsec. The resulting transverse resolution was then evaluated by measuring the cor-

responding LSF's. The loss in resolution observed while rejecting 50% or 75% of the photoelectrons from each γ-ray interaction is taken to be representative of that in a small 8×8 block which might eventually be modified for DOI sensitivity with L = 50% or L = 75% for γ's interacting at the median depth.

Figure 2(b) presents the LSF obtained for a crystal at the center of the small 8×8 block that has had no modifications for DOI sensitivity. The full line gives the LSF for an ADC integration time of 1000 nsec. The crystal response shows a FWHM of 4.5 mm and a much improved FWTM of 10 mm. The resulting LSF for $\Delta\tau$ = 190 (L=50%) is given by the dashed line. Compared to the nominal LSF, the FWHM remains the same while the FWTM degrades by not more than 1 mm and remains clearly better than that of 12×12 block. This indicates that the large FWTM of the depth sensitive 12×12 block is probably due to its finer (1/36) crystal segmentation as opposed to its reduced light collection efficiency.

Figure 2(c) presents the LSF obtained for a crystal at the center of the small 8×8 block using this time the pencil beam directed on its side face approximately at the median depth. The full line gives the LSF for an ADC integration time of 1000 nsec; the dashed line that with 190 nsec (L=50%); and the dotted line that with 80 nsec (L=75%). No difference is seen in the FWHM between fan and pencil beam data. With the pencil beam, the FWTM improves marginally to 9 mm for the nominal and 190 nsec integration times. This is presumably due to a reduced contribution from Compton scattered events in the pencil beam compared to the fan beam data. The LSF measured with $\Delta\tau$=80 nsec, corresponding to a L=75% loss in light collection efficiency at the median, remains better than that measured on the modified 12×12 block. This indicates that the significant reduction of the light collection efficiency required to achieve depth sensitivity will not destroy the transverse position resolution, provided the block segmentation is not too fine.

III. Simulation Outline

A Monte Carlo simulation was used to predict the performance of the complete DELAC based on the dimensions and resolutions of individual block candidates. It takes as its main inputs an energy resolution, $\Delta E/E$, a DOI sensitivity, S_{DOI}, and a crystal dependent set of LSF's.

Once the geometry of the tomograph has been initialised, events are randomly generated according to the specifications of a phantom source. The generation of each event follows the next steps:

- γ-ray pair generation;
- γ-rays tracking in the BGO;
- interactions blurring;
- Line-Spread-Functions smearing;
- DOI corrections;
- crystal addresses calculations;
- X-ray transform (i.e. sinogram binning) of LOR's;

Typically, for resolution studies, β-decays were generated in the volume of a small uniform spherical source somewhere in the camera's FOV. The source diameter was taken to be 1 mm to account for the range of positrons emerging from a point-like source. The relative angle between the momentum vectors of the emerging γ-rays is simulated as a gaussian distribution centered at 180° with a FWHM of 0.5° [5].

Both incoming γ's are then independently tracked in the BGO until a photoelectric interaction occurs in the volume of a block or they escape from it. The relative ratio of Compton to photoelectric cross-sections is used, as a function of energy, to randomly choose which of the two processes occurred. The flight path of the interacting γ is randomly generated according to the exponential attenuation based on interaction length. The total cross-section at the energy of the interacting γ determines the interaction length of the exponential distribution. For Compton interactions, the direction of the scattered γ follows the Klein-Nishina angular distribution. At each interaction vertex, i, the energy released, E_i, is firstly converted to an "apparent energy", E_i^a, according to the depth of that vertex; the linear DOI response of the block; and the ratio E_i/511 keV. The "apparent" energies of all interaction vertices are summed to yield the total energy, E^t, for the incident 511 keV γ. The total energy is converted into a "detected" energy, E^d, using a gaussian random smearing to account for the combined energy resolution of the PMT's. An energy resolution, $\Delta E/E$, representative of the block performance at the depth of maximum light collection efficiency is used. This resolution is degraded by $1/\sqrt{1-L}$ for each event to account for photon fractional loss. The photon fractional loss of the event, L, is evaluated by the ratio of E^t to the energy of a photoelectric event at the depth of maximum light collection efficiency in the block. The depth encoding features of the simulation may be turned off to simulate conventional tomograph performance.

The "interactions blurring" step then calculates the mean detection coordinates (X, Y, Z) of each incident γ. This is done by computing the centroid of all interaction vertices, each weighted by the ratio of its individual energy to the total, E_i^a/E^t.

Following the interaction blurring, the mean X- and Y-coordinates of each γ are smeared to account for position miscoding in the block. The mean X- and Y-coordinates resulting from the interaction blurring are used to identify an initial crystal for the interaction. The X- and Y-coordinates are then randomly redistributed to the center of the same or another crystal according to the probability distribution determined by the corresponding measured transverse LSF. The probability distribution is crystal-dependent and derived from measurements such as those

presented in Figure 2. Four-fold XY symmetry of the LSF's was assumed to simplify LSF's measurements. For the small 8×8 block, the photon fractional loss of the event, L, was used to reference the measured LSF's with either $\Delta\tau$ = 1000 nsec when $L \leq 33\%$; $\Delta\tau$ = 180 nsec when $33\% < L \leq 66\%$ or $\Delta\tau$ = 90 nsec when $L > 66\%$. This procedure is the most realistic simulation of the depth variation in transverse position miscoding possible given the existing small 8×8 block measurements. For the large 12×12 block the only set of LSF's available to the simulation are those measured after the block was modified.

Optionally, the X- and Y-coordinates can be corrected for the γ's DOI according to the method introduced by Moses *et al.* [6]. This method chooses the "most probable" DOI (MPDOI) between the front and back faces of the BGO block detector, given a measured DOI and its resolution. The linear DOI response of the block, is used to translate the detected energy, E^d, and its resolution into a measured DOI and its resolution. Each possible DOI along the block Z axis is assigned a likelihood. The likelihood is proportional to the exponential survival probability of 511 keV γ's at a possible DOI and to the gaussian probability that this depth yields the measured DOI given its resolution. The MPDOI is taken to be that for which the maximum likelihood is found. MPDOI values outside the block are not considered possible, so that shallow-interacting events, with poor energy or DOI resolution, pile up at the front face of the block. The corrections to the X- and Y-coordinates are calculated using the MPDOI and the direction cosines of the Line-Of-Response (LOR) that the uncorrected event makes at the surface of the block. The corrected X- and Y-coordinates are rounded to the nearest crystal center. If the DOI correction moves either coordinate outside the front face of the block, the center of the corresponding X- or Y-edge crystal is used. Switching off the DOI correction option of the simulation allows one to predict the impact of the DOI blurring on the resolution of either a conventional or a depth encoding tomograph operating without correction.

Optionally, the resulting X- and Y-coordinates can be uniformly smeared over the surface area of the final crystal. This removes binning artifacts arising from the rounding of the coordinates to crystal centers in the previous steps and is employed only if the final sinogram binning is finer than the widths of the distributions used in the LSF smearing.

The LOR connecting the final X- and Y-coordinates of both γ's is finally used to calculate the X-ray transform coordinates, (l_x, l_y, ϕ, θ) [7], of the event. Raw crystal and ring addresses are available as well. At this step acceptance cuts may also be applied if it is desired to analyse separately a subset of crystals, blocks or LOR's.

The reliability of the simulation was tested using experimental data. For instance simulated energy spectra agreed with the measured ones. The simulation simultaneously matched the measured ratio of Compton to photoelectric events, as well as the shapes of these two contributions.

Of utmost importance to the upcoming sections, the geometry of the septaless ECAT-953B [8] was simulated. Figure 3(a) compares, for a point source at the center of the FOV, the transaxial profile, called Point-Source-Projection (PSP), predicted by the simulation to a measured one under the same conditions. Experimental and simulated data were independently normalized to a unit area. The simulation is in very good agreement with the data and shows a PSP with a FWHM of 5 mm. Figure 3(b) compares simulated and measured PSP's, this time for a point source at 12 cm off center transaxially. Again, the simulation is in good agreement with the measured data. The shift and skewness of the PSP towards the center of the tomograph present in the data are well accounted for by the simulation.

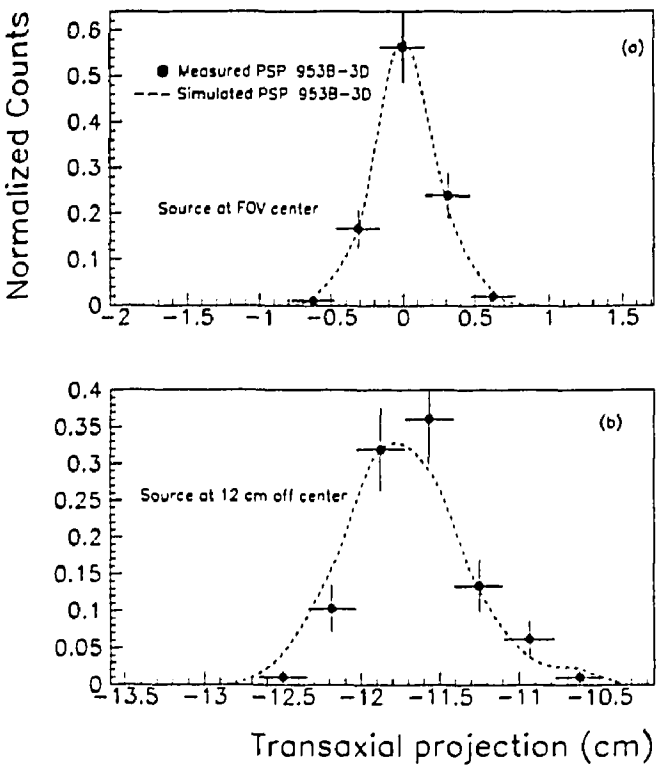

Figure 3: The measured (full circles) and simulated (dashed line) transaxial Point-Source-Projections (PSP's) for a source (a) at the center and (b) at 12 cm off center in the ECAT-953B with septa retracted.

IV. Results

A. *DELAC's Performance with the Large 12×12*

The simulation was initially used to predict the resolution of a DELAC of 43 cm ring radius and 10.8 cm axial extent, made of large 12×12 blocks. The characteristics of the existing 12×12 block that were presented in Figures 1 and 2(a) were used as input to the simulation described in the previous section. A uniform spherical source of 0.5 mm radius was simulated in the DELAC's FOV at transaxial

positions varying from the center to 25 cm off center, in steps of 5 cm. At each source position, transaxial profiles were formed for a projection view taken to be perpendicular to the direction of displacement of the source. The angular ϕ and θ ranges of the projection view were chosen to span half the full block acceptance on either side of the central LOR. This procedure averaged the different LSF's over all the crystals of a block. Such an averaging, called angular mashing [9], is routinely used to reduce the size of sinogram data sets. Here we use it to combine the effects of different crystal LSF's into one profile for ease of analysis. Typically 100 000 events were required in the projection view for a good statistical accuracy. The source projections were taken with and without using the DOI correction capacity of the block. Figure 4(a) presents the resulting PSP when the source is at the center of the FOV.

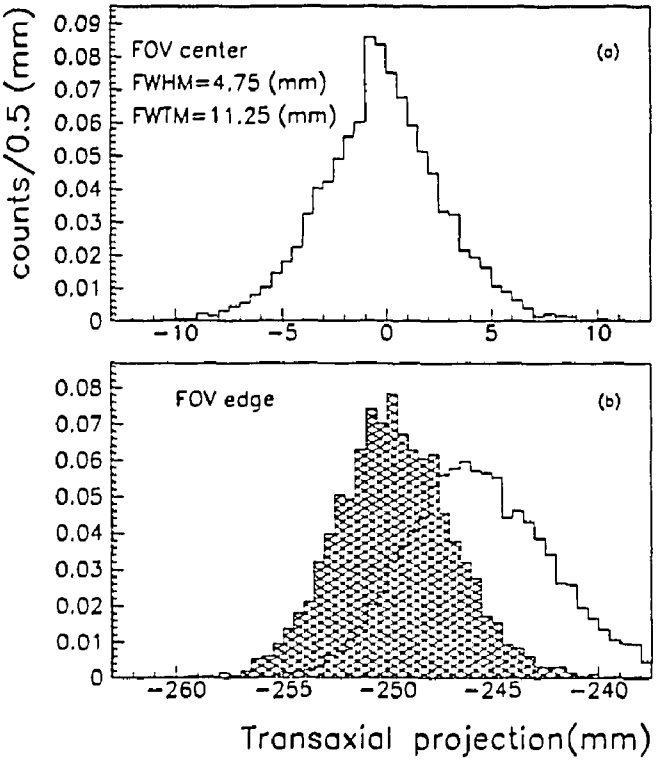

Figure 4: (a) Simulated transaxial projection for a spherical source of 0.5 mm radius at the center of the FOV in a DELAC made of large 12×12 blocks. (b) Simulated projections with (hatched histogram) and without (blank histogram) DOI correction when the same source is 25 cm from the FOV's center transaxially. The distributions are normalized to a unit area.

The PSP shows a FWHM (FWTM) of 4.75 mm (11.25 mm). This rather limited resolution was to be expected given the fine segmentation that degrades the LSF resolution presented in Figure 2(a).

Figure 4(b) presents the simulation results when the source is at 25 cm from the FOV's center transaxially. The unhatched histogram shows the projection obtained without correction for the γ's DOI. It is shifted toward the center of the FOV and skewed with a FWHM (FWTM) of 7.5 mm (14.5 mm). The hatched histogram shows the PSP obtained with the DOI correction. The corrected PSP is much improved compared to the uncorrected one. It is centered at the expected projection value in the X-ray transform coordinate system and symmetrical. The PSP resolution is worse than that at the center with a FWHM (FWTM) of 5.5 mm (12.0 mm). The depth resolution of the block allows a substantial recovery of the DOI blurring at the edges of the FOV.

B. Optimization with the small 8×8

The simulation was further used to assess the performance of a 41 cm ring radius, and 7.6 cm axial extent DELAC based on the better position resolution of the small 8×8 block. Hypothetical DOI sensitivities of $S_{DOI} = +75\%$, +50%, as well as $S_{DOI} = -75\%$ and -50% were assumed for 8×8 blocks of 36×38 mm. As already mentioned, the DOI sensitivity, S_{DOI}, quoted refers to the fraction of optical photons lost for γ's that interact at the top of the block. Hence, +75% (-75%) indicates that deep events will be 75% brighter (dimmer) than shallow ones. The thickness of the block, which affects its efficiency and the value of the median DOI, was also varied to 20 mm and 30 mm to assess the influence of this parameter on the DELAC resolution.

The DOI sensitivity, along with estimates of the resulting photon fractional loss, energy and DOI resolutions for γ's interacting at the median depth of the blocks are presented in Table 1 for hypothetical, 20 mm and 30 mm thick, small 8×8, block candidates. The energy resolution of the block at the median depth was evaluated using the measured resolution of $\Delta E/E = 21\%$ (FWHM) in the unmodified 8×8 block scaled by $1/\sqrt{1 - L(z_m)}$. The DOI resolution at the median follows from equation (7).

Apart from the block dimensions, and the energy resolution of 21%, the inputs to the simulation are the DOI sensitivity, along with the complete set of LSF's measured with the pencil beam as shown in Figure 2(c). Event-per-event evaluation of the energy and transverse position resolutions based on the photon fractional loss was used as described in the previous section.

The resolution obtained for a uniform point-like source at the center and at 25 cm from the center transaxially are given in Table 1. The FWHM and FWTM of the PSP's are those obtained for a spherical point-like source of 0.5 mm radius. All profiles were again taken from a projection view centered on a LOR perpendicular to the displacement of the source and spanning the acceptance of a block.

For a given DOI sensitivity, the PSP resolution at the center of the FOV is independent of the block thickness. However, at 25 cm the PSP resolution is better in the 20 mm thick block than in the 30 mm one. Because of the extra material in the 30 mm thick block, a significant number of γ's will interact in the last 10 mm of BGO. The

36 × 38 × 20 blocks, z_m=6.2 mm				
S_{DOI} (%)	+75	+50	-75	-50
$L(z_m)$ (%)	52	34	23	15
$\Delta E/E$ @ z_m (FWHM %)	30	26	24	23
$\Delta Z(z_m)$ (FWHM mm)	4	7	5	8
PSP FWHM(FWTM) @center	3.5(10.0)	3.5(9.0)	3.25(9.0)	3.25(9.0)
PSP^{corr} FWHM(FWTM) @25	4.0(9.5)	4.5(10.5)	4.5(10.0)	4.0(9.5)
36 × 38 × 30 blocks, z_m=7.9 mm				
S_{DOI} (%)	+75	+50	-75	-50
$L(z_m)$ (%)	55	37	20	13
$\Delta E/E$ @ z_m (FWHM %)	31	26	24	23
$\Delta Z(z_m)$ (FWHM mm)	6	10	8	12
PSP FWHM(FWTM) @center	3.75(10.0)	3.5(9.5)	3.5(9.5)	3.5(9.5)
PSP^{corr} FWHM(FWTM) @25	5.0(10.0)	5.0(10.5)	5.25(12.5)	4.5(12.5)

Table 1: Hypothetical 8×8 block specifications evaluated at the median depth of interaction z_m. The resulting Point-Source-Profile (PSP) resolution at the center and at 25 cm are given for a 41 cm ring radius DELAC.

parallax error of such events is large, causing a more severe DOI blurring that can only be partially corrected within the limited DOI resolution of the block.

For each block thickness, the corrected PSP resolution at 25 cm is better with a positive DOI sensitivity than with a negative one. This is particularly obvious at the FWTM level. The effect is more pronounced for large negative DOI sensitivities or for deeper blocks. Gamma's that Compton scatter at a shallow depth in the block and then escape through the side walls cause this degradation. For a negative DOI sensitivity, these shallow, low-energy events are incorrectly interpreted as deep events because of their small signal. The DOI correction moves the interaction point from its correct position at the front to an incorrect one nearer to the back face of the block, hence spoiling the resolution. The thicker the block, the larger the effect of this depth miscoding and the more severe will be the blurring. In a realistic source environment, depth miscoding of object-scattered gammas is expected to lead to a similar degradation.

Accordingly, the best resolution performance is expected for a DELAC based on the 20 mm deep block candidate with S_{DOI} = +75%. For that block, the resolution at the center of the DELAC is expected to be of 3.5 mm (10.0 mm) FWHM (FWTM). At 25 cm of the FOV's center it is predicted to be of 4.0 mm (9.5 mm) FWHM (FWTM) with the DOI correction.

C. *Resolution Uniformity in a DELAC*

Figure 5 presents the predicted variation of the PSP FWHM and FWTM as a function of the source offset from the FOV's center in cameras of 41 cm (left) and 31 cm (right) ring radius. The full squares give the resolution of a "conventional" camera made of unmodified, 20 mm thick, small 8×8 blocks. The full triangles give the predicted resolution after the DOI correction in a DELAC made of the best small 8×8 block candidates, 20 mm thick and with S_{DOI} = +75%. The error of ±0.25 mm on the profile resolution accounts for the uncertainty in extracting the FWHM and FWTM from projections with 0.5 mm wide bins.

The advantages and disadvantages of the depth encoding blocks in a conventional camera geometry are well illustrated by the PSP resolution obtained with a ring radius of 41 cm. Comparing the performance of the unmodified blocks to the depth encoding ones, the simulation indicates a loss of resolution in the central region of the DELAC's FOV, especially at the FWTM level. This loss is attributable to the increased tails of the LSF's in the DOI sensitive blocks with their reduced light collection efficiency. As expected, the loss due to the depth sensitivity is less severe in the FWHM. At the center, the FWHM of the PSP is maintained in the DOI sensitive blocks. There, the DOI of incident γ-rays and extra position miscoding have a negligible impact on the resolution which is dominated by the crystals' transaxial dimension.

The simulation also indicates that the DOI correction is effective only if the source is offset by more than ~12 cm from the center. The DOI correction to the transverse coordinates of an event depends on the depth as well as on the ratio of the source position, x_s, to the ring radius, R. Because the coordinates are rounded to the nearest crystal center, the correction must also be larger than $\pm 1/2$ the crystal width to cause an effect. As a result, only outside the radius where this is satisfied for most events, is the PSP resolution of the DELAC better than that of the conventional design.

When the source is 25 cm from the center transaxially, the PSP FWHM (FWTM) is predicted to be 4.0 mm (9.5 mm) in the DELAC compared to 5.75 mm (11.75) in the camera made of conventional blocks. Although the expected depth resolution of the block is not sufficient to completely recover the loss due to DOI blurring, there

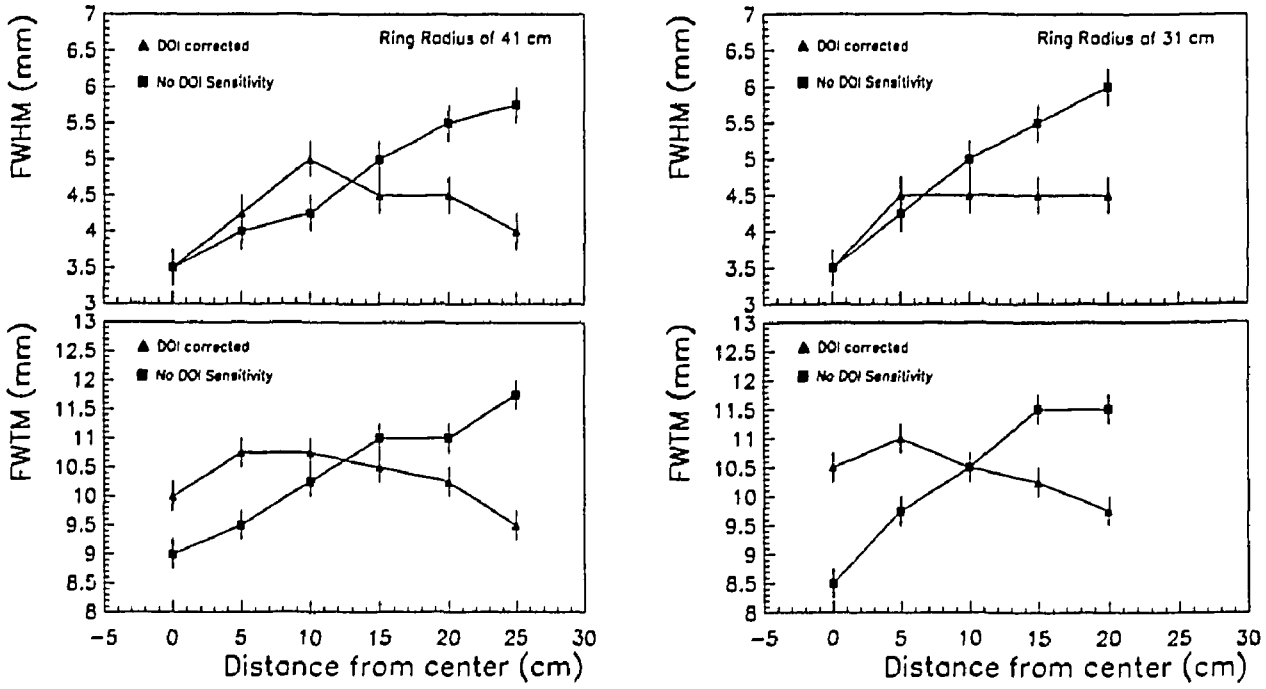

Figure 5: Predicted variation of the PSP FWHM (top) and FWTM (bottom) as a function of the source offset from the FOV's center in cameras of 41 cm (left) and 31 cm (right) ring radius. The full squares give the resolution predicted for a camera made of unmodified, 20 mm thick, small 8×8 blocks. The full triangles give the resolution after the DOI correction in a DELAC made of 20 mm thick, small 8×8 blocks with $S_{DOI} = +75\%$.

will be a gain of ~2 mm in resolution at the edge of the DELAC's FOV. Overall the PSP FWHM and FWTM will both be more uniform in the DELAC than in the conventional camera.

The simulation results obtained for a "small" ring radius of 31 cm, shown on the right of Figure 5, emphasize even better the possible gain in resolution uniformity in a depth encoding camera compared to one made of conventional blocks. The disadvantages that were highlighted for the 41 cm ring radius DELAC are present. There is a degradation of the DELAC's PSF FWTM in the inner part of the FOV, while its PSP FWHM is less affected. But, due to the $1/R$ dependence of the DOI correction, the depth sensitivity of the block has a stronger impact on the resolution at given source position. As a result, the DOI correction becomes effective at a source position closer to the FOV's center. Therefore, the uniformity of the PSP resolution in a DELAC of smaller ring radius is superior.

V. Discussion and Conclusions

The results that were obtained in this first feasibility study of the DELAC, a wholebody PET tomograph with the capacity to correct for DOI blurring, are very encouraging. The measured performances of the large 12×12 block clearly indicate that a good DOI sensitivity can be achieved by a suitable modification of the surface treatment in standard BGO position encoding detectors for PET. The resolution measurements made on the small 8×8 block further support that DOI sensitivity can be obtained with reduced light collection efficiency without spoiling the transverse position resolution of the block. Indeed, narrowing the width of the ADC integration time to reduce uniformly the collected photoelectrons by half did not impact significantly on the transverse position resolution. A significant degradation appears when as much as 3/4 of the photoelectrons are cut. Hence, it seems that the cost in light collection efficiency paid to acquire DOI sensitivity can be afforded without sacrificing the transverse resolution, at least up to a loss of one half of the total light available. However, from the unsatisfactory position resolution of the 12×12 block, this seems to be true only provided that the block is not too finely segmented. *The light available per photoelectric event can be used either for finer transverse segmentation of the block or for DOI sensitivity, but not both simultaneously.*

In spite of its unsatisfactory transverse resolution, the performance of the large 12×12 block is sufficient alone to demonstrate its ability to correct for the parallax error using the DOI information of the block. This initial proof of principle was based on extrapolating with a Monte Carlo simulation the measured performances of that block to a conventional size wholebody tomograph of 43 cm ring radius. For a point-like source at the edge of the FOV, the corrected projection is much improved compared to the uncorrected one. The correction moves the projection to

its expected coordinate and removes the tail towards the FOV center. The corrected projection shows a resolution of 5.5 mm FWHM and 12.0 mm FWTM, which is to be compared to 4.75 mm and 11.25 mm at the center.

The search for the block specifications and DELAC ring radius that would optimize the resolution quality and uniformity across the FOV leads to interesting conclusions as to what extent one can correct for the parallax error. Best results were obtained assuming that a DOI sensitivity of $S_{DOI} = +75\%$ can be achieved in a 20 mm deep small 8×8 block. The comparison of a DELAC made of those blocks to a camera made with conventional blocks showed that the loss in light collection efficiency degrades the PSP resolution at the FWTM level, in the inner part of the DELAC's FOV. The effect is less prominent on the FWHM. At the edge of the FOV, the DOI correction improves clearly the point source resolution to 4.0 mm (9.5 mm) FWHM (FWTM) in the DELAC as compared to 5.75 mm (11.75) in the conventional camera. The DOI corrected PSP resolution remains worse at the edge of the FOV than at the center. Compton scattering in the BGO, which is not correctable, is believed to be the source of this limitation.

Because of the rounding of the transverse coordinates to the crystal centers, the ratio of the source position to the ring radius, x_s/R, needs to be sufficiently large for the DOI correction to be effective. The $1/R$ dependence of the correction was shown to result in a better resolution uniformity if the ring of the DELAC is made smaller than that of the current generation of wholebody PET tomographs. This result leads to the conclusion that the availability of depth encoding blocks, as specified in this study, would make possible the design of PET cameras with better image resolution and sensitivity at reduced cost. The achieved resolution uniformity across a wide FOV would further enlarge the range of clinical applications for this modality.

To confirm the feasibility of such a depth encoding camera, a systematic investigation of the combined effect of the ring radius, detection threshold, block thickness and DOI sensitivity on the "object" and "detector" scatter contributions is now needed.

Two parameters can significantly effect the scatter fraction in the DELAC, namely the ring radius and the detection threshold. Reducing the ring radius increases the acceptance to object scatters and true events both with typically a $1/R$ dependence. The fraction of object scattered to total events shows only a gradual increase with shrinking ring radius [10], but is not expected to be dramatically higher in a 31 cm radius DELAC than in existing state-of-the-art septaless tomographs. The energy threshold will also impact on the scatter fraction. In a depth sensitive block, this threshold must be set to reject signals that are lower than the lowest possible photopeak ADC channel considering the DOI sensitivity and energy resolution of the block. The threshold effectively varies depending on the DOI of the γ's. For example, in a block with positive DOI sensitivity, the rejection of scattered events is less effective if they interact deeper. This may also, as a result, lead to larger scatter fraction in a DELAC.

The influence of scatters on the DOI corrected resolution is also of fundamental importance. To understand the impact of scattered events on the position resolution in DOI sensitive blocks, one must consider the depth distribution of these events in the BGO, the value and sign of S_{DOI}, and the effect of the DOI correction on their initial depth distribution. Object scatters undergo a stronger attenuation in BGO due to their reduced energy. As a result, they tend to interact in the first centimeter of the block and deposit little energy. For positive DOI sensitivity, these events are characterized by a low detected signal and are correctly interpreted as shallow interactions. The DOI correction moves these events towards the front face of the block by a small relative amount in depth. It has little effect on them and they accordingly do not further degrade the PSP resolution. On the contrary, for a negative DOI sensitivity, the same shallow low energy events may incorrectly be interpreted as deep photoelectric interactions because of their low signal. The DOI correction then effectively moves them from the front towards the back face of the block, which degrades the resolution. Blurring of the resolution due to depth miscoding of scatter events could be partially avoided by raising the detection threshold, but would reduce the detection efficiency. From that point of view, a positive DOI sensitivity therefore seems preferable.

Finally, measurements on a pair of DOI sensitive blocks are ongoing in the continuation of this work. Such measurements will allow us to compare the resolution of standard and DOI sensitive blocks in a realistic object scatter environment and hopefully confirm on experimental grounds the feasibility of a Depth Encoding Large Aperture Camera.

VI. Acknowledgements

We are thankful to B. Evans, R. R. Johnson, R. Moore, K. S. Morrison and V. Sossi for helpful discussions and their participation in the first phase of the DELAC project at TRIUMF which has motivated this work.

This study would also not have been possible without the collaboration of Ronald Nutt, M. Andreaco and C. W. Williams of Siemens-CTI, where our detector candidates were fabricated. We also thank Dr. Simon Cherry of UCLA for loaning us the two 8×8 blocks he received from CTI.

We wish to acknowledge the support of the Medical Research Council of Canada.

Christian Moisan acknowledges the Natural Sciences and Engineering Research Council of Canada for its support through a postdoctoral fellowship.

REFERENCES

[1] J. G. Rogers, "A method for correcting the Depth-of-Interaction blurring in PET cameras", to appear in IEEE Trans. Med. Imag. (in press).

[2] J. G. Rogers, A. J. Taylor, M. F. Rahimi, R. Nutt, M. Andreaco and C. W. Williams, "An improved multicrystal 2-D BGO detector for PET", IEEE Trans. Nucl. Sci., **NS-39** 1063 (1992).

[3] J.G.Rogers, R.Nutt, M.Andreaco and C.W.Williams, "Testing 144- and 256-crystal BGO block detectors", IEEE Trans. Nucl. Sci., **NS-41** 1423 (1994).

[4] W. W. Moses and S. E. Derenzo, "Design studies for a PET detector module using a PIN photodiode to measure depth of interaction.", IEEE Trans. Nucl. Sci., **NS-41** 1441 (1994).

[5] C. J. Thompson, J. Moreno-Cantu and Y. Picard, "PETSIM: Monte Carlo simulation of all sensitivity and resolution parameters of cylindrical positron imaging systems", Phys. Med. Biol., **37**, No. 3, 731 (1992).

[6] W. W. Moses, R. H. Huesman and S. E. Derenzo, "A new algorithm for using Depth-of-Interaction measurement information in PET data acquisition", J. Nucl. Med., **32** 995 (1991).

[7] P. E. Kinahan, J. G. Rogers, R. Harrop, and R. R. Johnson, "Three-dimensional image reconstruction in object space", IEEE Trans. Nucl. Sci., **NS-35** 635 (1988).

[8] T.J. Spinks, T. Jones, D. L. Bailey, D. W. Townsend, S. Grootoonk, P. M. Bloomfield, M.-C. Gilardi, M. E. Casey. B. Sipe and J. Reed, "Physical performance of a positron tomograph for brain imaging with retractable septa", Phys. Med. Biol., **37**, No. 8, 1637 (1992).

[9] H. P. Gadagkar and M. E. Casey, "Investigating the effect of angular mashing of PET sinogram data on reconstructed images", 1993 IEEE MIC Conference Record, Vol. 2, 1213-1216 (1993).

[10] M. Dahlbom, S. R. Cherry, L. Eriksson, E. J. Hoffman, K. Weinhard, "Optimization of PET instrumentation for brain activation studies", IEEE Trans. Nucl. Sci., **NS-40** 1048 (1993).